EE5705 Electric Drives in Sustainable Energy Systems Course Project 3

Pei Xu

May 14, 2016

1 Introduction

Doubly fed induction generators (DFIGs) are a kind of induction machines, who is widely used in wind generation. The major advantage of DFIG is its sufficiently wide speed range, which is able to make the combined wind turbine run at the optimum coefficient of performance C_p^{opt}.

This report focuses on the modeling of DFIG with a combined wind turbine in dq domain and the modeling of controllers based on dq domain, as described in Chapter 3, 5 and 7 in [2].

The report is organized as the following. First, a detailed mathematical model of induction machines in dq domain is provided. Then, the report, based on the characteristics of DFIG, offers a modification to the general mathematical model and provides the vector control model of DFIG. And, a basic model for the wind turbine and its torque controller is provided then. Finally, a set of simulation is conducted, in order to test the performance of the designed controllers.

2 General Mathematical Model of Induction Machine in dq Domain

2.1 Assumptions

Similarly to Project 1, the study to the model of induction machines are based on the below assumptions.

- The airgap is uniform.
- Eddy currents, friction and windage losses are all negligible.
- Stator and rotor windings are identical.
- The studied induction machine works under the condition in which the magnetic fields are unsaturated.
- The studied induction machine is magnetic linear.

- The studied induction machine has a squirrel-cage rotor.
- The input voltages and currents of the studied induction machine are sinusoidal balanced.

2.2 dq Winding Representation

For stator windings, in three-phase frame, assuming phase a is the reference phase, the stator current space vector $\vec{i}_s$ and the magnetomotive force space vector $\vec{F}_s$ at time t are defined as

$$\vec{i}_s^a(t) = i_a(t) + i_b(t)e^{j2\pi/3} + i_c(t)e^{j4\pi/3} \tag{2.1}$$

and

$$\vec{F}_s^a(t) = \frac{N_s}{p}\vec{i}_s^a(t) \tag{2.2}$$

where $i_a(t)$, $i_b(t)$ and $i_c(t)$ are the phase currents of the stator windings at time t, N_s is the equivalent turns of each stator winding, and p is the number of poles.

Supposing that the magnetomotive force at any instant time is produced by a group of two orthogonal windings, i_{sd} and i_{sq}, each of which has kN_s equivalent turns, then we have

$$\frac{kN_s}{p}(i_{sd}(t) + j\ i_{sq}(t)) = \frac{N_s}{p}\vec{i}_s^d(t) \tag{2.3}$$

where $\vec{i}_s^d$ is $\vec{i}_s$ using d-axis as the reference axis and is obtained as

$$\vec{i}_s^d(t) = \vec{i}_s^a(t)e^{-j\theta_{da}(t)} \tag{2.4}$$

in which $\theta_{da}(t)$ is the intersection angle between d-axis and a-axis at time t in electrical space.

Here we choose

$$k = \sqrt{3/2} \tag{2.5}$$

such that the winding magnetizing inductance in the dq domain satisfies

$$dq \text{ winding magnetizing inductance} = k^2 L_{m,1\phi} = L_m \tag{2.6}$$

where L_m is the per-phase magnetizing inductance in the three-phase frame, $L_{m,1\phi}$ is single-phase magnetizing inductance that is the same in both stator and rotor based on the assumptions.

Therefore, i_{sd} and i_{sq} can be obtained as

$$i_{sd} = \sqrt{\frac{2}{3}} \times Re\{\vec{i}_s^d(t)\} \tag{2.7}$$

and

$$i_{sq} = \sqrt{\frac{2}{3}} \times Im\{\vec{i}_s^d(t)\} \tag{2.8}$$

where $Re\{\vec{i}_s^d(t)\}$ and $Im\{\vec{i}_s^d(t)\}$ are respectively the real and imaginary part of $\vec{i}_s^d(t)$; and thus the relationship between dq currents and abc currents can be expressed as

$$\boldsymbol{i}_{s,dq} = \boldsymbol{T}_{s,abc\to dq}\boldsymbol{i}_{s,abc} \tag{2.9}$$

$$\boldsymbol{i}_{s,abc} = \boldsymbol{T}_{s,dq\to abc}\boldsymbol{i}_{s,dq} \tag{2.10}$$

where $\boldsymbol{i}_{s,abc} = \begin{bmatrix} i_a(t) \\ i_b(t) \\ i_c(t) \end{bmatrix}$, $\boldsymbol{i}_{s,dq} = \begin{bmatrix} i_{sd}(t) \\ i_{sq}(t) \end{bmatrix}$, $\mathbf{T_{s,abc\to dq}}$ and $\mathbf{T_{s,dq\to abc}}$ are the transformation matrices for stator windings that are obtained as

$$\boldsymbol{T}_{s,abc\to dq} = \sqrt{\frac{2}{3}} \begin{bmatrix} \cos(\theta_{da}(t)) & \cos(\theta_{da}(t) - 2\pi/3) & \cos(\theta_{da}(t) + 2\pi/3) \\ -\sin(\theta_{da}(t)) & -\sin(\theta_{da}(t) - 2\pi/3) & -\sin(\theta_{da}(t) + 2\pi/3) \end{bmatrix} \tag{2.11}$$

and

$$\boldsymbol{T}_{s,dq\to abc} = \sqrt{\frac{2}{3}} \begin{bmatrix} \cos(\theta_{da}(t)) & -\sin(\theta_{da}(t)) \\ \cos(\theta_{da}(t) - 2\pi/3) & -\sin(\theta_{da}(t) - 2\pi/3) \\ \cos(\theta_{da}(t) + 2\pi/3) & -\sin(\theta_{da}(t) + 2\pi/3) \end{bmatrix} \tag{2.12}$$

Similarly, for stator voltages, we have

$$\boldsymbol{v}_{s,dq} = \boldsymbol{T}_{s,abc\to dq}\boldsymbol{v}_{s,abc} \tag{2.13}$$

and

$$\boldsymbol{v}_{s,abc} = \boldsymbol{T}_{s,dq\to abc}\boldsymbol{v}_{s,dq} \tag{2.14}$$

where $\boldsymbol{v}_{s,dq} = \begin{bmatrix} v_{sd}(t) \\ v_{sq}(t) \end{bmatrix}$ and $\boldsymbol{v}_{s,abc} = \begin{bmatrix} v_a(t) \\ v_b(t) \\ v_c(t) \end{bmatrix}$.

For rotor windings, we have

$$\boldsymbol{i}_{r,dq} = \boldsymbol{T}_{r,ABC\to dq}\boldsymbol{i}_{r,ABC}, \quad \boldsymbol{v}_{r,dq} = \boldsymbol{T}_{r,ABC\to dq}\boldsymbol{v}_{r,ABC} \tag{2.15}$$

and

$$\boldsymbol{i}_{r,ABC} = \boldsymbol{T}_{r,dq\to ABC}\boldsymbol{i}_{r,dq}, \quad \boldsymbol{v}_{r,ABC} = \boldsymbol{T}_{r,dq\to ABC}\boldsymbol{v}_{r,dq} \tag{2.16}$$

where $\boldsymbol{i}_{r,dq} = \begin{bmatrix} i_{rd}(t) \\ i_{rq}(t) \end{bmatrix}$, $\boldsymbol{v}_{r,dq} = \begin{bmatrix} v_{rd}(t) \\ v_{rq}(t) \end{bmatrix}$, $\boldsymbol{i}_{r,ABC} = \begin{bmatrix} i_A(t) \\ i_B(t) \\ i_C(t) \end{bmatrix}$, $\boldsymbol{v}_{r,ABC} = \begin{bmatrix} v_A(t) \\ v_B(t) \\ v_C(t) \end{bmatrix}$,

$$\boldsymbol{T}_{r,ABC\to dq} = \sqrt{\frac{2}{3}} \begin{bmatrix} \cos(\theta_{dA}(t)) & \cos(\theta_{dA}(t) - 2\pi/3) & \cos(\theta_{dA}(t) + 2\pi/3) \\ -\sin(\theta_{dA}(t)) & -\sin(\theta_{dA}(t) - 2\pi/3) & -\sin(\theta_{dA}(t) + 2\pi/3) \end{bmatrix} \tag{2.17}$$

and

$$\boldsymbol{T}_{r,dq\to ABC} = \sqrt{\frac{2}{3}} \begin{bmatrix} \cos(\theta_{dA}(t)) & -\sin(\theta_{dA}(t)) \\ \cos(\theta_{dA}(t) - 2\pi/3) & -\sin(\theta_{dA}(t) - 2\pi/3) \\ \cos(\theta_{dA}(t) + 2\pi/3) & -\sin(\theta_{dA}(t) + 2\pi/3) \end{bmatrix} \tag{2.18}$$

in which $\theta_{dA}(t)$ is the intersection angle between d-axis and A-axis at time t in electrical space.

2.3 Flux Leakage Equation

Given that dq windings are orthogonal, there is no mutual inductance between d and q windings. Therefore, for stator windings, due to that the leakage flux caused by rotor currents does not cross the air gap, we have

$$\lambda_{sd} = (L_{ls} + L_m)i_{sd} + L_m i_{rd} \tag{2.19}$$

and

$$\lambda_{sq} = (L_{ls} + L_m)i_{sq} + L_m i_{rq} \tag{2.20}$$

where L_{ls} is the stator leakage inductance.

Similarly, for rotor windings, we have

$$\lambda_{rd} = (L_{lr} + L_m)i_{rd} + L_m i_{sd} \tag{2.21}$$

and

$$\lambda_{rq} = (L_{lr} + L_m)i_{rq} + L_m i_{sq} \tag{2.22}$$

where L_{lr} is the rotor leakage inductance.

Combining the above four equations, we obtain the flux leakage equation

$$\begin{bmatrix} \boldsymbol{\lambda}_{s,dq} \\ \boldsymbol{\lambda}_{r,dq} \end{bmatrix} = \begin{bmatrix} L_s & 0 & L_m & 0 \\ 0 & L_s & 0 & L_m \\ L_m & 0 & L_r & 0 \\ 0 & L_m & 0 & L_r \end{bmatrix} \begin{bmatrix} \boldsymbol{i}_{s,dq} \\ \boldsymbol{i}_{r,dq} \end{bmatrix} \tag{2.23}$$

where $L_s \triangleq L_{ls} + L_m$, $L_r \triangleq L_{lr} + L_m$ and $\boldsymbol{\lambda}_{s,dq} = \begin{bmatrix} \lambda_{sd}(t) \\ \lambda_{sq}(t) \end{bmatrix}$, $\boldsymbol{\lambda}_{r,dq} = \begin{bmatrix} \lambda_{rd}(t) \\ \lambda_{rq}(t) \end{bmatrix}$.

2.4 Voltage Equation

According to Ohm's law and Faraday's law, the stator voltage space vector can be expressed as

$$\vec{v}_s^a = R_s \vec{i}_s^a + \frac{d}{dt}\vec{\lambda}_s^a \tag{2.24}$$

where R_s is the equivalent resistance of each stator winding.

Therefore, we have

$$\vec{v}_s^d e^{j\theta_{da}} = R_s \vec{i}_s^d e^{j\theta_{da}} + \frac{d}{dt}(\vec{\lambda}_s^d e^{j\theta_{da}}) \tag{2.25}$$

Simplifying the above equation, we get

$$\begin{aligned} \vec{v}_s^d &= R_s \vec{i}_s^d + \frac{d\vec{\lambda}_s^d}{dt} + j\vec{\lambda}_s^d \frac{d\theta_{da}}{dt} \\ &= R_s \vec{i}_s^d + \frac{d\vec{\lambda}_s^d}{dt} + j\omega_d \vec{\lambda}_s^d \end{aligned} \tag{2.26}$$

where

$$\omega_d = \frac{d\theta_{da}}{dt} \tag{2.27}$$

Given that $\vec{v}_s^d = v_{sd} + j\ v_{sq}$, $\vec{i}_s^d = i_{sd} + j\ i_{sq}$ and $\vec{\lambda}_s^d = \lambda_{sd} + j\ \lambda_{sq}$ we have

$$\boldsymbol{v}_{s,dq} = R_s \boldsymbol{i}_{s,dq} + \frac{d}{dt}\boldsymbol{\lambda}_{s,dq} + \omega_d \begin{bmatrix} 0 & -1 \\ 1 & 0 \end{bmatrix} \boldsymbol{\lambda}_{s,dq} \tag{2.28}$$

Similarly, for rotor windings, we have

$$\boldsymbol{v}_{r,dq} = R_r \boldsymbol{i}_{r,dq} + \frac{d}{dt}\boldsymbol{\lambda}_{r,dq} + \omega_{dA} \begin{bmatrix} 0 & -1 \\ 1 & 0 \end{bmatrix} \boldsymbol{\lambda}_{r,dq} \tag{2.29}$$

where R_r is the equivalent resistance of each stator winding and

$$\omega_{dA} = \frac{d\theta_{dA}}{dt} \tag{2.30}$$

2.5 Torque Equation

Given that dq windings are orthogonal, the produced torque on the d-axis is caused by the the flux that is due to the q-axis winding. Referring to Chapter 10 of [1], we have

$$dT_{em,d}(\xi) = \left[\frac{p}{2} \cdot r \cdot (\widehat{B}_{rq} \cos\xi) \cdot l \cdot i_{rd} \cdot (\frac{\sqrt{3/2}N_s}{p} \cos\xi) \right] d\xi \tag{2.31}$$

where $\widehat{B}_{rq} \cos\xi$ is the flux density caused by rotor windings on q-axis at angle ξ, r is the rotor radius, and l is the length of rotor.

Therefore,

$$T_{em,d} = 2 \int_{\xi=-\pi/2}^{\xi=\pi/2} dT_{em,d}(\xi) = \frac{p}{2} \left(\pi \frac{\sqrt{3/2}N_s}{p} r l \widehat{B}_{rq} \right) i_{rd} \tag{2.32}$$

Given that $\widehat{B}_{rq} = \mu_0 \widehat{H}_{rq} = \mu_0 \frac{\widehat{F}_{rq}}{l_g}$, $\widehat{F}_{rq} = \left(\frac{\sqrt{3/2}N_r}{p} \right) \frac{\lambda_{rq}}{L_m}$ and $N_r = Ns$ where μ_0 is the permeability of air, l_g is the length of air gap, $\widehat{H}_{rq}$ is the peak filed intensity of rotor windings along the q-axis, $\widehat{F}_{rq}$ is the peak magnetomotive force of rotor windings along the q-axis, N_r is the equivalent turns of each rotor winding, and N_s is the equivalent turns of each stator winding, the above equation can be further simplied, and $T_{em,d}$ can be expressed as

$$T_{em,d} = \frac{p}{2}(L_m i_{sq} + L_r i_{rq}) i_{rd} = \frac{p}{2} \lambda_{rq} i_{rd} \tag{2.33}$$

Similarly, the produced torque on the q-axis can be expressed as

$$T_{em,q} = -\frac{p}{2}(L_m i_{sd} + L_r i_{rd}) i_{rq} = -\frac{p}{2} \lambda_{rd} i_{rq} \tag{2.34}$$

Therefore, the electromagnetic torque can be expressed as

$$T_{em} = T_{em,d} + T_{em,q} = \frac{p}{2}(\lambda_{rq} i_{rd} - \lambda_{rd} i_{rq}) \tag{2.35}$$

or

$$T_{em} = \frac{p}{2} L_m (i_{sq} i_{rd} - i_{sd} i_{rq}) \tag{2.36}$$

2.6 Angular Equations

The intersection angle between a-axis and A-axis in electrical radians, θ_m, satisfies

$$\theta_{dA} = \theta_{da} - \theta_m \tag{2.37}$$

$$\frac{d}{dt}\theta_{dA} = \omega_{dA} \tag{2.38}$$

and

$$\theta_m = \int \omega_m(t)dt + \theta_0 \tag{2.39}$$

where ω_m is the electrical rotational speed and θ_0 is the the initial angle by which rotor and stator coils are offset in electrical space.

Therefore, according to Eqn. 2.27 and 2.30 we have

$$\omega_d = \omega_{dA} + \omega_m \tag{2.40}$$

Based on the assumptions, we have

$$\frac{d\omega_{mech}}{dt} = \frac{T_{em} - T_L}{J} \tag{2.41}$$

where ω_{mech} is the mechanically rotational speed and T_L is the load torque and J is the moment of inertia.

Given that

$$\omega_m = \frac{p}{2}\omega_{mech} \tag{2.42}$$

where p is the number of poles of the given induction machine, we have the angular acceleration equation

$$\frac{d\omega_m}{dt} = \frac{p}{2}\frac{T_{em} - T_L}{J} \tag{2.43}$$

3 dq Model for DFIGs

3.1 Assumptions

Besides the assumptions described in Section 2.1, the model of DFIG is also based on the following assumptions:

- The stator voltage is applied by the power grid with balanced sinusoidal three phase voltage.
- The rotor voltage is controllable through power electronics.
- The stator and rotor leakage inductances and resistances are quite small and even negligible.

3.2 Selection of d-Axis

Due to that the stator voltage is applied by the power grid and thus is uncontrollable, the purpose of modeling DFIGs in dq domain is to control DFIG (its speed, electromagnetic torque and so on) through the two decoupling axial components of rotor current or voltage in dq domain. Usually, the d-axis is chosen to be aligned with the rotor flux-leakage space vector or the direction stator voltage. In this project, the direction of the stator voltage $\vec{v}_s^a$ is chosen as the d-axis.

When the d-axis is aligned with $\vec{v}_s^a$, we have the following equations

$$|\vec{v}_s^a| = v_{s,d} \tag{3.44}$$

$$v_{s,q} = 0 \tag{3.45}$$

$$\theta_{da} = \angle \vec{v}_s^a \tag{3.46}$$

i.e.

$$\vec{v}_s^a = v_{s,d} \angle \theta_{da} \tag{3.47}$$

and the rotational speed of d-axis is equal to the rotational speed of $\vec{v}_s$ in electrical space, i.e.

$$\omega_d = \omega_{\vec{v}_s} \tag{3.48}$$

Let $\vec{v}_s^a = v_\alpha + j v_\beta$. Given that the stator voltage is applied by the power grid balanced sinusoidal three phase voltage $v_a \angle 0°$, $v_b \angle 120°$ and $v_c \angle$-120°, we have

$$v_\alpha = v_a \cos 0° + v_b \cos 120° + v_b \cos(\text{-}120°) \tag{3.49}$$

and

$$v_\beta = v_a \sin 0° + v_b \sin 120° + v_b \sin(\text{-}120°) \tag{3.50}$$

Writing Eqn. 3.49 and 3.50 in the form of matrix, we can obtain

$$\begin{bmatrix} v_\alpha \\ v_\beta \end{bmatrix} = \begin{bmatrix} 1 & -\frac{1}{2} & -\frac{1}{2} \\ 0 & \frac{\sqrt{3}}{2} & \frac{\sqrt{3}}{2} \end{bmatrix} \begin{bmatrix} v_a \\ v_b \\ v_c \end{bmatrix} = \begin{bmatrix} \sqrt{\frac{2}{3}} \widehat{V}_s \\ 0 \end{bmatrix} \tag{3.51}$$

where $\widehat{V}_s$ is the peak value of the phase voltage applied to the stator. According to $\vec{v}_s^a = v_{s,d} \angle \theta_{da}$, we have

$$\theta_{da} = \tan^{-1} \frac{v_\beta}{v_\alpha} \tag{3.52}$$

and

$$\omega_d = \omega_{syn} = 2\pi f_{syn} \tag{3.53}$$

where f_{syn} is the frequency of the grid.

Given that for DFIGs, the stator resistances are quite small, we have

$$Rs \approx 0 \tag{3.54}$$

And, in steady state,

$$\frac{d}{dt} \boldsymbol{\lambda}_{s,dq} \approx 0 \tag{3.55}$$

Therefore, from Eqn. 2.28, in steady state, we have

$$v_{sd} \approx \text{-}\omega_d \lambda_{sq} \tag{3.56}$$

and

$$v_{sq} \approx \omega_d \lambda_{sd} \tag{3.57}$$

i.e.

$$\lambda_{sq} \approx \text{-}\frac{v_{sd}}{\omega_d} \tag{3.58}$$

and

$$\lambda_{sd} \approx \frac{v_{sq}}{\omega_d} \tag{3.59}$$

Given that $v_{sq} = 0$, we have

$$\lambda_{sd} \approx 0 \tag{3.60}$$

Given that $\lambda_{sd} = L_m i_{rd} + L_s i_{sd}$, we have

$$i_{sd} \approx \text{-}\frac{L_m}{L_s} i_{rd} \tag{3.61}$$

3.3 Selection of Control Variables

Given that the stator real and reactive power can be obtained as

$$P_s + jQ_s = (v_{sd} + jv_{sq})(i_{sd} + ji_{sq})^H \tag{3.62}$$

where the superscript H denotes the conjugate of the given complex-valued vector, we have

$$P_s = v_{sd} i_{sd} + v_{sq} i_{sq} \tag{3.63}$$

$$Q_s = v_{sq} i_{sd} - v_{sd} i_{sq} \tag{3.64}$$

Similarly, for the rotor real and reactive power $P_r + jQ_r = (v_{rd} + jv_{rq})(i_{rd} + ji_{rq})^H$, we have

$$P_r = v_{rd} i_{rd} + v_{rq} i_{rq} \tag{3.65}$$

$$Q_r = v_{rq} i_{rd} + v_{rd} i_{rq} \tag{3.66}$$

Given that $v_{sq} = 0$ and $i_{sd} \approx \text{-}\frac{L_m}{L_s} i_{rd}$, we have

$$P_s = v_{sd} i_{sd} \approx -\frac{L_m}{L_s} v_{sd} i_{rd} \tag{3.67}$$

Given that $v_{sq} = 0$ and $\lambda_{sq} = L_m i_{rq} + L_s i_{sq} \approx -\frac{v_{sd}}{\omega_d}$, we have

$$Q_s = -v_{sd} i_{sq} \approx v_{sd}(\frac{v_{sd}}{\omega_d L_s} + \frac{L_m}{L_s}) i_{rq} \tag{3.68}$$

Given that $\lambda_{sq} = L_s i_{sq} + L_m i_{rq} \approx -\frac{v_{sd}}{\omega_d}$, $\lambda_{sd} = L_m i_{rd} + L_s i_{sd}$, $\lambda_{sd} \approx 0$, $\lambda_{sq} \approx -\frac{v_{sd}}{\omega_d}$ and $i_{sd} \approx$ -$\frac{L_m}{L_s} i_{rd}$, we have

$$\begin{aligned} T_{em} &= \tfrac{p}{2} L_m (i_{sq} i_{rd} - i_{sd} i_{rq}) \\ &= \tfrac{p}{2} \tfrac{L_m}{L_s} [(\lambda_{sq} - L_m i_{rq}) i_{rd} - (\lambda_{sd} - L_m i_{rd}) i_{rq}] \\ &\approx -\tfrac{p L_m v_{sd}}{2 \omega_d L_s} i_{rd} \end{aligned} \tag{3.69}$$

Given that $v_{sd} = \sqrt{\frac{2}{3}} \widehat{V}_s$ is a constant, from Eqn. 3.67, 3.68 and 3.69, it can be recognized that we can control the DFIG's stator real power P_s and electromagnetic T_{em} through adjusting i_{rd} and control the DFIG's stator reactive power Q_s through adjusting i_{rq}. In summary, the d-axis rotor current is employable to control the stator active power as well as the electromagnetic torque and the q-axis rotor current is employable to control the stator flux as well as the stator reactive power. Obviously, it is able to control the DFIG through the two decoupling components i_{rd} and i_{rq}, and our control purpose is reachable.

The reference signal can be obtained from the desired electromagnetic torque (or the desired stator real power) and the desired stator reactive power, as shown below

$$i_{rd}^* \approx -\frac{L_s}{L_m v_{sd}} P_s^* \tag{3.70}$$

$$i_{rd}^* \approx -\frac{2 L_s \omega_d}{p L_m v_{sd}} T_{em}^* \tag{3.71}$$

$$i_{rq}^* \approx -\frac{L_s v_{sd}}{L_m L_s \omega_d} + \frac{L_s}{L_m v_{sd}} Q_s^* \tag{3.72}$$

3.4 Controller Design for DFIG

In the control strategy mentioned in the last subsection, i_{rd} and i_{rq} is chosen as the reference signals, and the input signals to the DFIG model is $\boldsymbol{v}_{r,abc}$, which can be calculated from v_{sd} and v_{sq}.

From Eqn. 2.29, and $\frac{d}{dt} \boldsymbol{\lambda_{r,dq}} = 0$, the d- and q-axis rotor voltages can be expressed as the summuation of two components, as shown below

$$v_{rd} = \underbrace{R_r i_{rd} + \sigma L_r \frac{d}{dt} i_{rd}}_{v'_{rd}} \underbrace{-\omega_{dA} \sigma L_r i_{rq}}_{v_{rd,comp}} \tag{3.73}$$

$$v_{rq} = \underbrace{R_r i_{rq} + \sigma L_r \frac{d}{dt} i_{rq}}_{v'_{rq}} + \underbrace{\omega_{dA} \sigma L_r i_{rd}}_{v_{rq,comp}} \tag{3.74}$$

where

$$\sigma \triangleq 1 - \frac{L_m^2}{L_s L_r} \tag{3.75}$$

From

$$\boldsymbol{v}'_{r,dq} = R_r \boldsymbol{i}_{r,dq} + \sigma L_r \frac{d}{dt} \boldsymbol{i}_{r,dq} \tag{3.76}$$

where $\boldsymbol{v}'_{r,dq} = \begin{bmatrix} v'_{rd} \\ v'_{rq} \end{bmatrix}$, we have

$$\boldsymbol{i}_{r,dq}(s) = \frac{1}{R_r + s\sigma L_r} \boldsymbol{v}'_{r,dq}(s) \tag{3.77}$$

in which s is the complex number frequency parameter.

According to Eqn. 3.77, the applied voltages v_{sd} and v_{sq} can be obtained via the current loop whose transfer function is

$$K_i(s) = \frac{1}{R_r + s\sigma L_r} \tag{3.78}$$

Here, we adopt a PI controller whose transfer function is

$$K_i(s) = \frac{K_{i,i}}{s} + K_{p,i} \tag{3.79}$$

And, we can develop the expressions for $K_{i,i}$ and $K_{p,i}$ as

$$K_{i,i} = \omega_c^2 \sqrt{\frac{R_r^2 + (\omega_c L_r \sigma)^2}{\omega_c^2 + \tan^2(PM - \pi/2 + \arctan(\omega_c L_r \sigma / R_r))}} \tag{3.80}$$

and

$$K_{p,i} = \frac{K_{i,i} \tan(PM - \pi/2 + \arctan(\omega_c L_r \sigma / R_r))}{\omega_c} \tag{3.81}$$

where PM is the desired phase margin and ω_c is the desired crossover frequency. A more detailed discussion of the PI controller design is provided in [1].

Due to that the voltage we obtain from the PI control is $\boldsymbol{v}'_{r,dq}$ rather than $\boldsymbol{v}_{r,dq}$, we need a voltage compensator for the applied voltage v_{rd} and v_{rq}. The compensation can be calculated from

$$\boldsymbol{v}_{r,dq,comp} = \omega_{dA} \sigma L_r \begin{bmatrix} 0 & -1 \\ 1 & 0 \end{bmatrix} \boldsymbol{i}_{r,dq} \tag{3.82}$$

where $\boldsymbol{v}_{r,dq,comp} = \begin{bmatrix} v_{rd,comp} \\ v_{rq,comp} \end{bmatrix}$.

4 Modeling of Wind Turbine

4.1 Mathematical Model of Wind Turbine

Similarly to the induction machine, for a wind turbine, we have

$$\frac{d\omega_{mech}}{dt} = \frac{T_{turb} - T_{em,gen}}{J_{turb}} \tag{4.83}$$

where ω_{mech} here is the mechanically rotational speed of the wind turbine, T_{turb} is the output torque of the wind turbine, $T_{em,gen}$ is the electromagnetic torque of the generator combined with the wind turbine and J_{turb} is the moment of inertia of the system composed of the wind turbine and the combined generator.

For a wind turbine, its output power is associated with T_{turb}, as shown below

$$P_{out} = P_{turb} = T_{turb}\omega_{mech} \tag{4.84}$$

and its input power is associated with the speed of wind, as shown below

$$P_{in} = P_{wind} = \frac{1}{2}\rho A v_{wind}^3 \tag{4.85}$$

where ρ is the destiny of air whose unit is $\mathrm{kg/m^3}$ and A is the swept area whose unit is $\mathrm{m^2}$.

The relationship between P_{turb} and P_{wind} can be expressed as

$$P_{turb} = C_p P_{wind} = C_p \frac{1}{2}\rho A v_{wind}^3 \tag{4.86}$$

where C_p is the wind power coefficient that is defined as

$$C_p = \frac{P_{out}}{P_{in}} \tag{4.87}$$

Therefore, T_{turb} can be expressed as

$$T_{turb} = C_p \frac{1}{2}\rho A \frac{R^3}{\lambda^3}\omega_{wind}^2 \tag{4.88}$$

For a given wind turbine, its wind power coefficient C_p usually is a function of v_{wind}/ω_{mech} and *beta* where v_{wind} is wind speed and *beta* in general is a constant. Therefore, C_p can be regarded as a function of v_{wind}/ω_{mech}. Define the tip-speed radio (TSR) as

$$\lambda = \frac{R\omega_{mech}}{v_{wind}} \tag{4.89}$$

C_p can be further regarded as a function of λ. The plot of C_p versus λ usually has the shape as shown in Fig. 1.

For $C_p = C_p^{opt}$, the corresponding TSR is represented as λ^{opt}, i.e. $C_p(\lambda^{opt}) = C_p^{opt}$. The relationship between λ^{opt} and ω_{mech}^{opt} can be expressed as

$$\lambda^{opt} = \frac{R\omega_{mech}^{opt}}{v_{wind}} \tag{4.90}$$

where λ^{opt} usually is a constant for a given wind turbine and ω_{mech}^{opt} usually is dependent on wind speed v_{wind}.

For a given wind speed, the plot of C_p versus ω_{mech} is shown in Fig.2. From the figure, we can find that there exists a value of ω_{mech} at which C_p has the maximum value. Let C_p^{opt} denote the maximum value of C_p, and let ω_{mech}^{opt} denote the corresponding value of ω_{mech}.

When the wind turbine operates, we hope the wind power coefficient C_p can keep at C_p^{opt} such that the wind turbine has the maximum efficiency to convert the input power into the output power. In other words, we hope the mechanically rotational speed of the wind power, ω_{mech}, can keep at ω_{mech}^{opt} who usually would change according to wind speed.

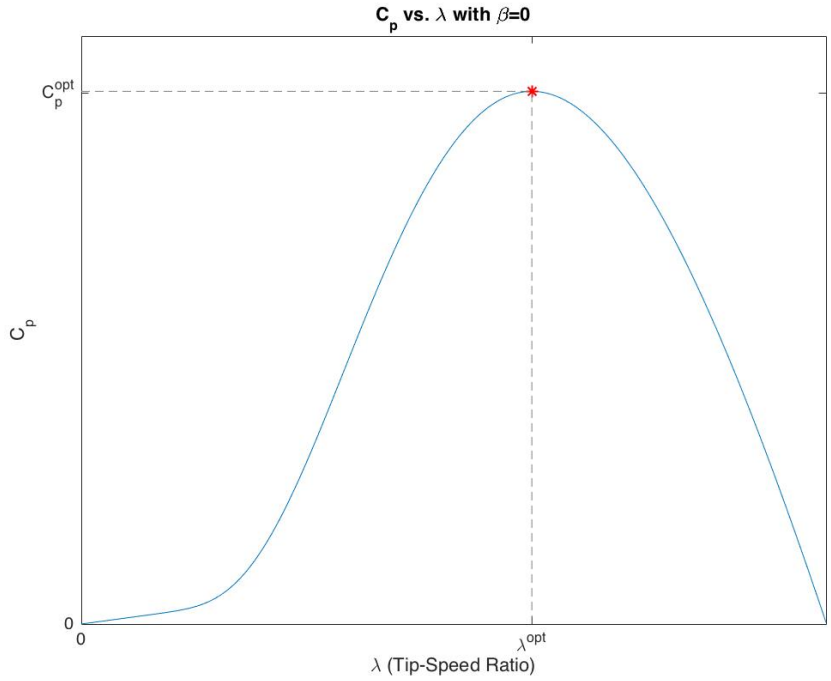

Figure 1: The Shape of the Wind Power Coefficient C_p versus Tip-Speed Ratio λ

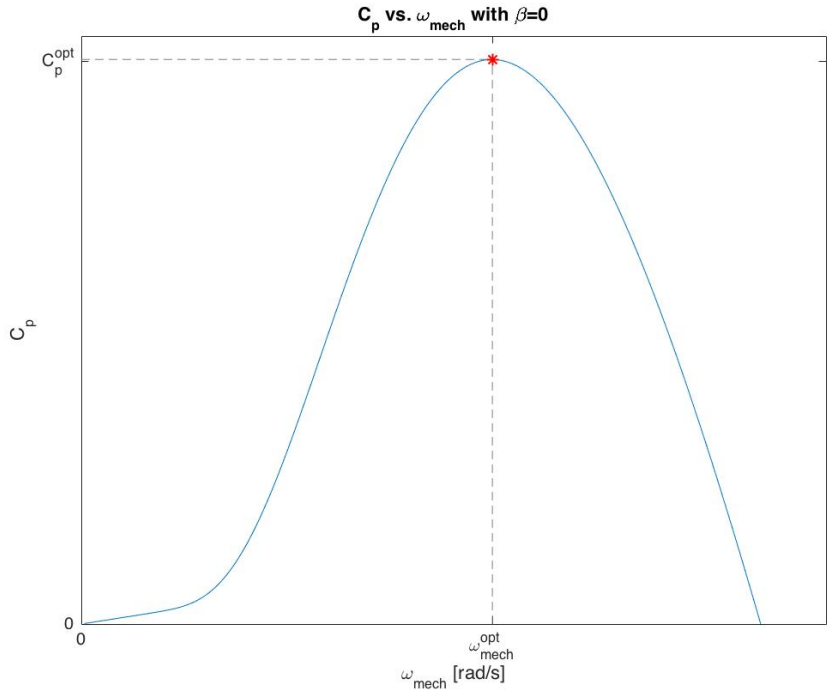

Figure 2: The Shape of the Wind Power Coefficient C_p versus the Mechanically Rotational Speed ω_{mech}

4.2 Speed-Squared Controller for Wind Turbine

Given Eqn. 4.83, ω_{mech} is controllable through adjusting $T_{em,gen}$. Here we adopt a speed-squared controller to generate the reference signal $T^*_{em,gen}$.

Due to that we hope the wind turbine runs with the maximum wind power coefficient C_p^{opt}, similarly to Eqn. 4.88, the reference signal of $T_{em,gen}$ can be obtained as

$$\begin{aligned} T^*_{em,gen} &= \frac{C_p^{opt}\rho A R^3}{2\lambda^{opt}}\omega^2_{mech} \\ &= K_{opt}\omega^2_{mech} \end{aligned} \tag{4.91}$$

Therefore, the controller used to generate the reference signal of $T_{em,gen}$ can be expressed as

$$K_{opt} = C_p^{opt}\frac{1}{2}\rho A\frac{R^3}{\lambda^{opt}} \tag{4.92}$$

who is a proportional controller whose input signal is ω^2_{mech} and whose output signal is T^*_{em}.

4.3 Combination of Wind Turbine and DFIG

The DFIG is combined with the wind turbine through a gearbox. The electromagnetic torque is amplified by a given ratio and then affects on the wind turbine as $T_{em,gen}$. The system performs in the accordance with Eqn. 4.83. ω_{mech} of the wind turbine as the output is amplified by the given ratio and then affects on the DFIG as the mechanically rotational speed of the DFIG. In this combined system, the model of the wind turbine produces T_{turb} according to the parameters of the turbine and wind speed. This process is described via Eqn. 4.88. The details of the combination of the DFIG and wind turbine is shown in Fig. 8.

5 Case Study

5.1 Modeling of DFIG Combined with Wind Turbine in MATLAB/Simulink

The MATLAB/Simulink model of the studied DFIG in *dq* domain is shown in Fig. 3.

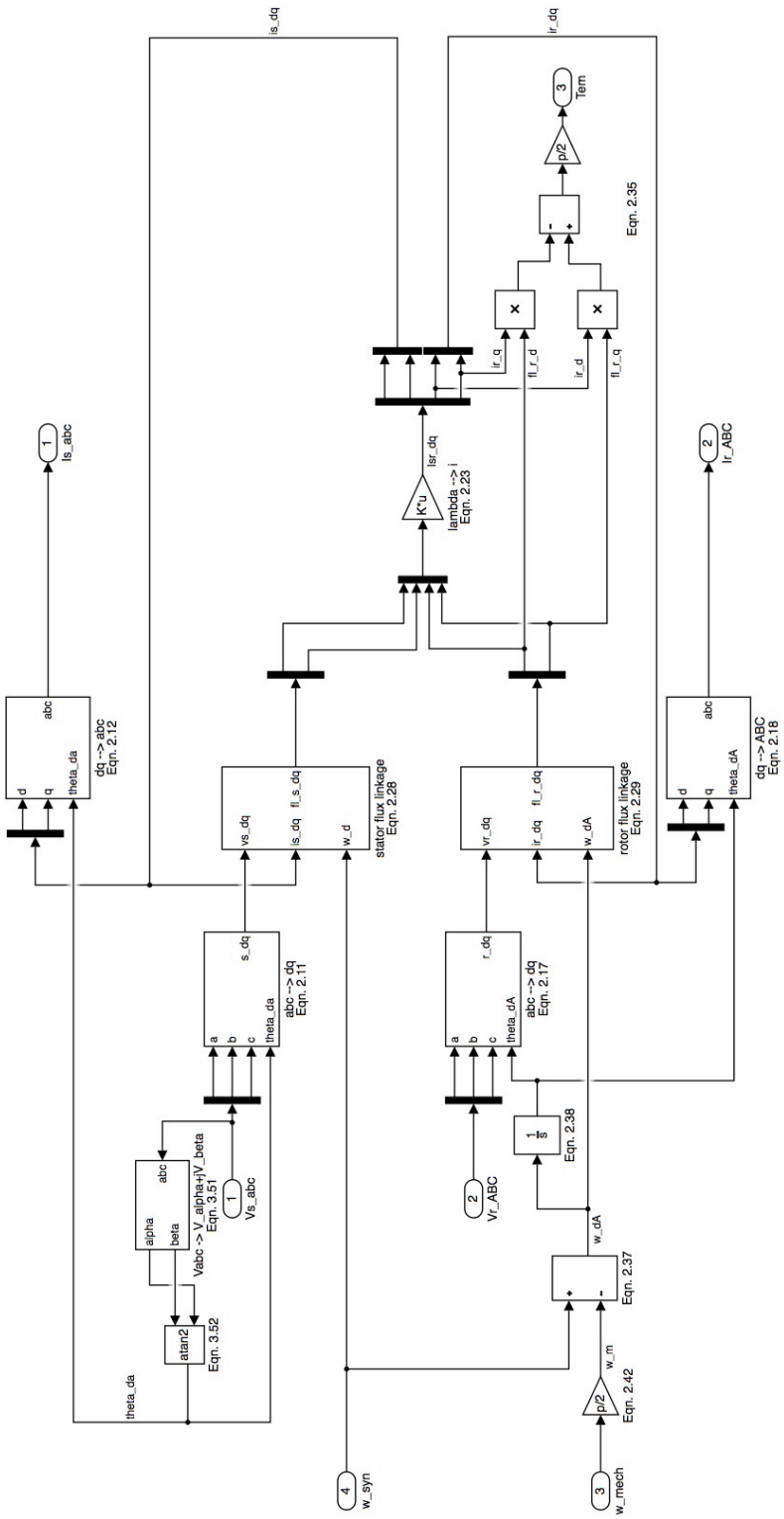

Figure 3: Model of DFIG in dq Domain

The estimator model, who calculates $\boldsymbol{v}_{s,dq}$, $\boldsymbol{i}_{s,dq}$, $\boldsymbol{v}_{r,dq}$ and $\boldsymbol{i}_{r,dq}$ all of which can be used as the feedback signal for the controller and who calculates ω_{dA} and θ_{dA} which are used for the rotor voltage compensation model and for the calculation of the applied rotor voltage in three-phase frame from the voltage in dq domain, is shown in Fig. 4. Bascially, this estimator model is similar to the DFIG model except for that there is no need to calculate the current and torque in the estimator model.

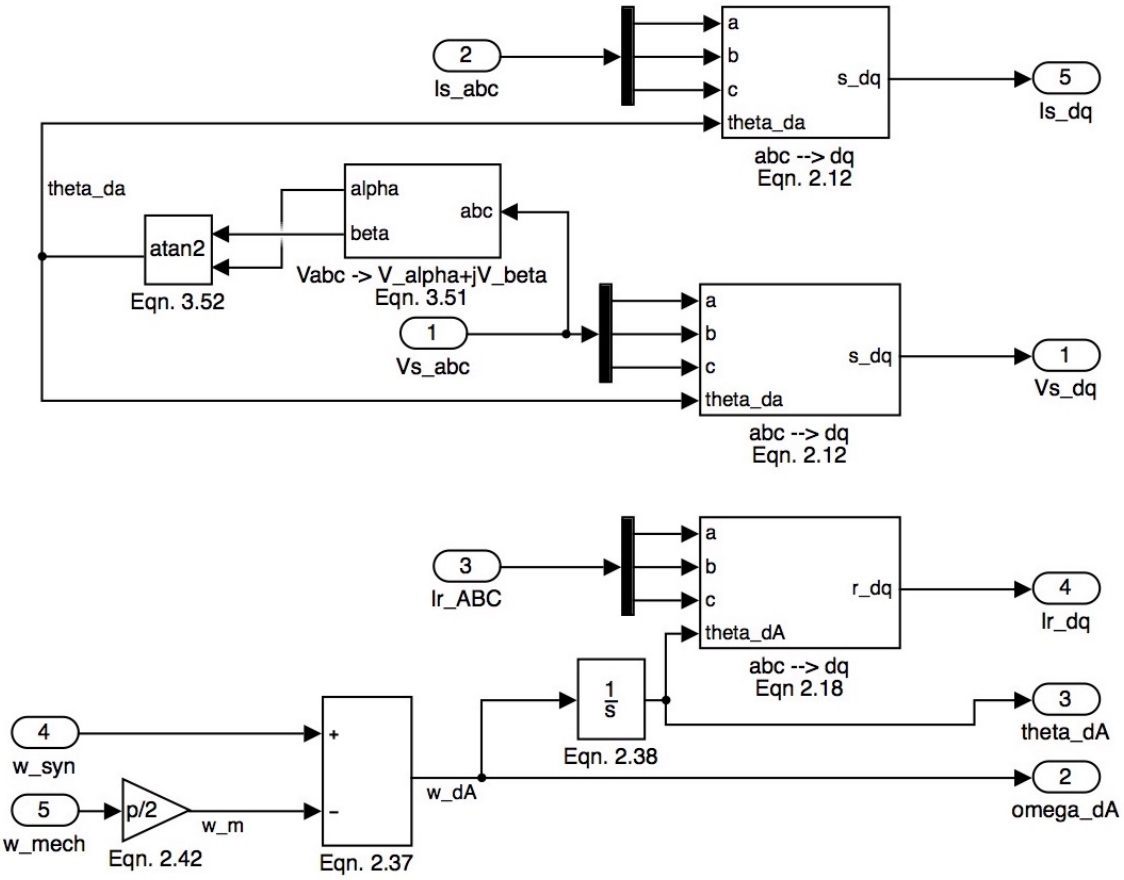

Figure 4: Model of Estimator Model

The detail of the DFIG controller and rotor voltage compensation model is shown in Fig. 5.

For the controller, the reference signal i_{rq}^* is controlled through adjust the reference signal Q_s^*, while the reference signal i_{rd}^* is controlled directly. The process of generating i_{rq}^* from Q_s^* is shown in Fig. 6

The model of the studied wind turbine is shown in Fig. 7.

The DFIG and wind turbine is combined in the form shown in Fig. 8. The stator voltage

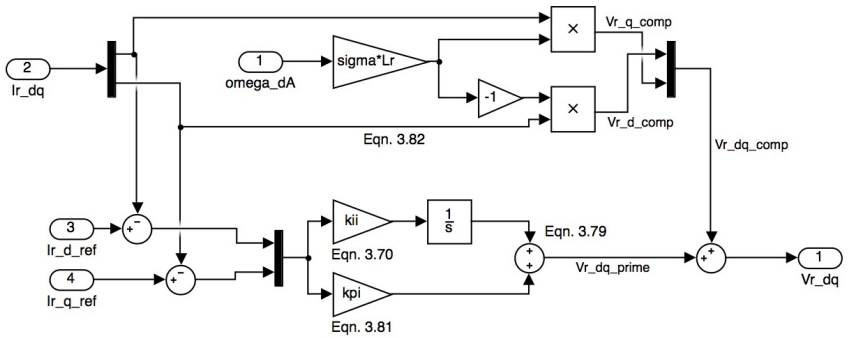

Figure 5: Model of the DFIG Controller with Rotor Voltage Compensation

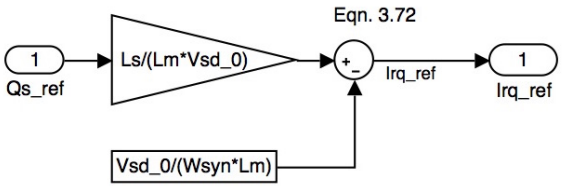

Figure 6: Model of Generating i_{rq}^* from Q_s^*

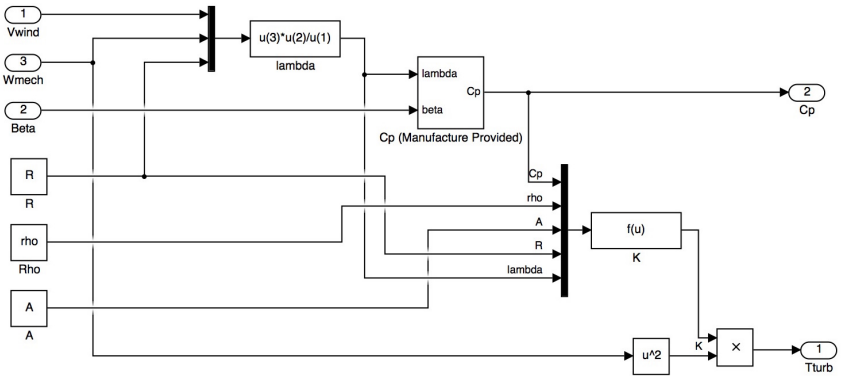

Figure 7: Model of the Studied Wind Turbine

applied to the DFIG is balanced sinusoidal three-phase voltage, which satisfies that

$$\begin{aligned}\overline{V}_a &= v_\phi^{rated}\angle 0^\circ \\ \overline{V}_b &= v_\phi^{rated}\angle 120^\circ \\ \overline{V}_c &= v_\phi^{rated}\angle \text{-}120^\circ\end{aligned} \tag{5.93}$$

where v_ϕ^{rated} is the rated phase voltage. The applied rotor voltage is calculated from v_{rd} and v_{rq} obtained from the controller in Fig. 5. The gear ratio is set as

$$GearRatio = \frac{\omega_{mech}^{rated}}{\omega_{mech}^{opt}} \tag{5.94}$$

where $\omega_{mech}^{rated} = (1-s)\omega_{syn}/(p/2)$ is the rated mechanically rotational speed of the DFIG and s is the slip of the DFIG at full (rated) load, and ω_{mech}^{opt} is obtained from the given C_p model at $v_{wind} = 12$ m/s. The detail of the speed-squared controller is shown in Fig. 9.

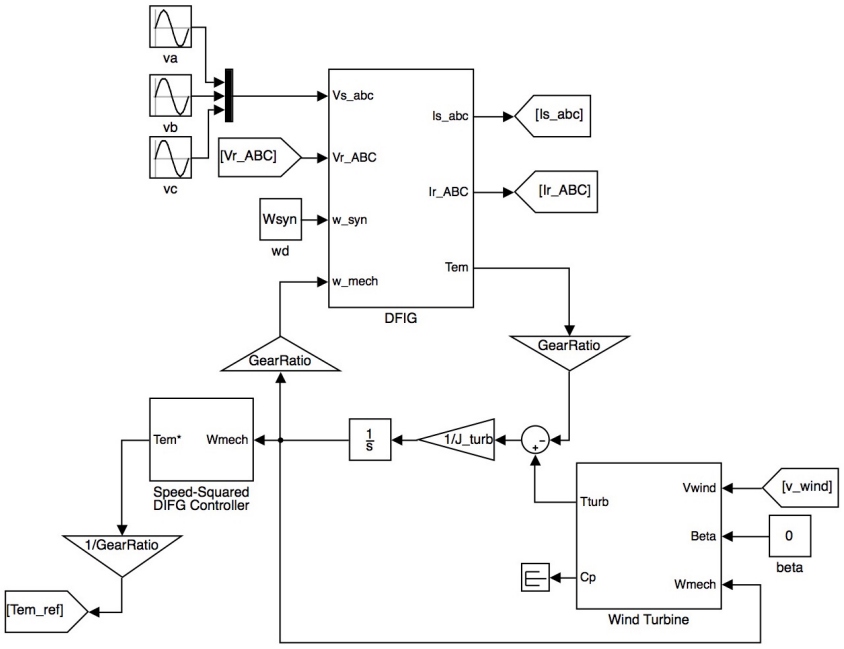

Figure 8: Combination of the DFIG and the wind turbine

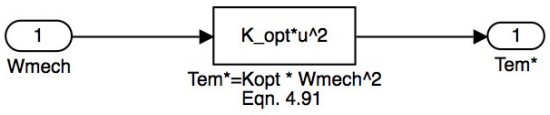

Figure 9: Model of the Speed-Squared Controller for the Wind Turbine

We employ Eqn. 3.71 to generate the reference signal of i_{rd} from T_{em}^* generated via the speed-squared controller. The detail of generating i_{rd}^* is shown in Fig. 10.

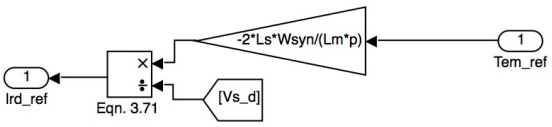

Figure 10: Model of Generating the Reference Signal i_{rd}^*

5.2 Simulation and Numerical Analysis

5.2.1 Specifications of the Studied DFIG and Wind Turbine

The studied DFIG is based on an example provided in [2], while the studied wind turbine is based on a GE wind turbine. The involved specifications of the DFIG are listed in Table 1 and the specifications of the wind turbine are listed in Table 2.

Table 1: Specifications of the Studied DFIG

Rated Line Voltage (RMS Value)	690 V	R_s	2.0 mΩ
Rated Frequency	$f_{syn} = 60$ Hz	R_r	1.5 mΩ
Poles	$p = 6$	X_{ls}	50 mΩ
Full Load Slip	$s = 1\%$	X_{lr}	47 mΩ
Moment of Inertia	$J = 75$ kg·m^2	X_m	860 mΩ

Table 2: Specifications of the Studied Wind Turbine

Swept Area	A = 3904 m^2	Rotor Diameter	2R = 70.5 m
Density of Air	$\rho = 1.2$ kg/m^3	System Inertia	$J_{turb} = 2.4 \times 10^6$ kg·m^2

5.2.2 Simulation for DFIG Controller Performance

In this simulation, we only exam the performance of the DFIG controller shown in Fig. 5 and do not combine the wind turbine with the DFIG. The simulation starts from the rated state of DFIG. Then the reference signal, i_{rd}^*, from the rated value of i_{rd} directly decreases to $i_{rd}/2$ at time $t = 0.1$ s; the reference signal, Q_s^*, from the rated value of Q_s directly decreases to 0 at time $t = 0.5$ s.

The simulation results are shown in Fig. 11, 12 and 13.

As described in the last section, the control of i_{rd} is realized through directly controlling the reference signal i_{rd}^*, while the control of i_{rq} is realized through controlling the reference signal Q_s^*. From Fig. 11 and 12, we can spot that the controller described in Section 3.4 can effectively adjusting i_{rd} and i_{rq}. Besides, from the two figure, it can be recognized that although the change in one of i_{rd} and i_{rq} could cause the fluctuation of the other one, the fluctuation is very limited and thus the two quantities basically are decoupling. That is to say, we can control P_s and Q_s dependently through adjusting i_{rd} and i_{rq} respectively.

In Fig. 13, the actual value T_{em} is the electromagnetic torque generated by the DFIG; the

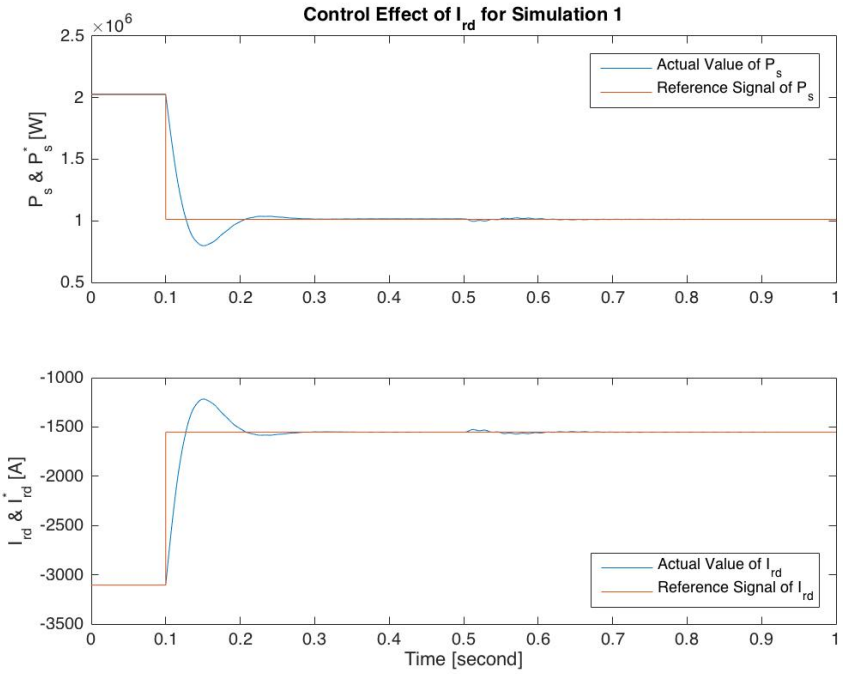

Figure 11: Simulation Results of the Control Effect of i_{rd} for Simulation 1

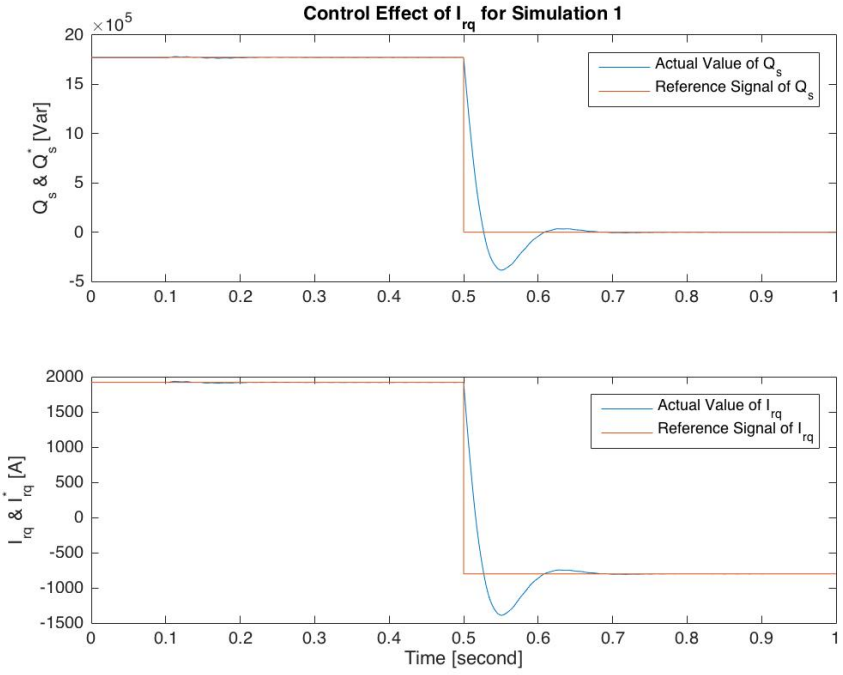

Figure 12: Simulation Results of the Control Effect of i_{rq} for Simulation 1

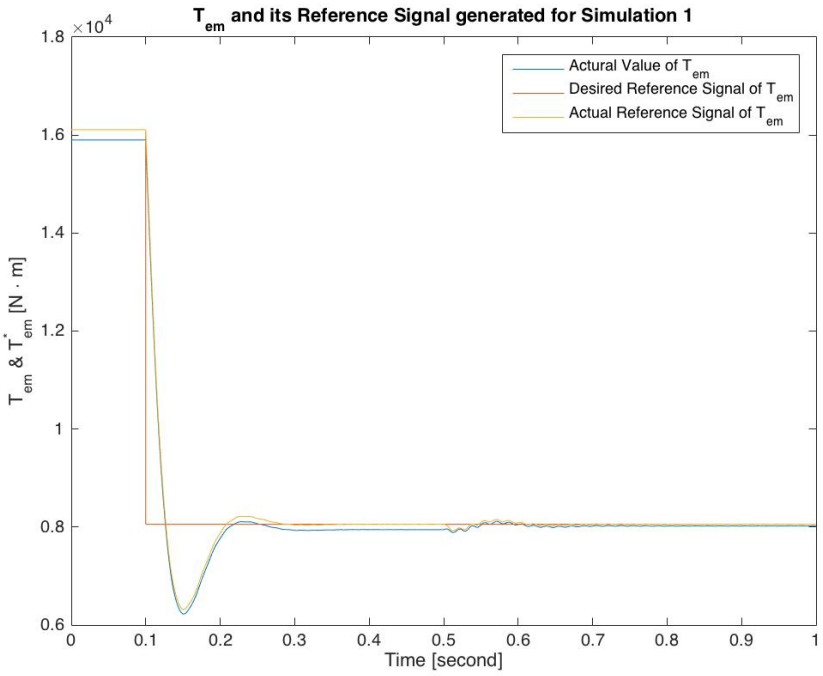

Figure 13: Simulation Results of the Control Performance of T_{em} for Simulation 1

desired reference signal is calculated via

$$T^*_{em,1} \approx -\frac{pL_m v_{sd}}{2\omega_d L_s} i^*_{rd} \tag{5.95}$$

which is the value that we hope T_{em} to be, while the actual reference signal is calculated via

$$T^*_{em,2} \approx -\frac{pL_m v_{sd}}{2\omega_d L_s} i_{rd} \tag{5.96}$$

which is the actual reference signal the model generated.

From Fig. 13, we can find that in steady state $T^*_{em,1}$ is identical to $T^*_{em,2}$ basically and that in dynamic state $T^*_{em,2}$ is more close to $T^*_{em,1}$ compared to T_{em}. This means the actually generated reference signal meet our desire. Besides, it can be spotted that there is a gap between the actual electromagnetic torque and the desired value. This is caused by the losses of approximation in the calculation of T^*_{em}.

5.2.3 Simulation for Speed-Squared Controller Performance

In this simulation, we assume that the DFIG always is able to generate the desired electromagnetic torque, i.e. $T_{em,gen} = T^*_{em}$, and thus we can evaluate the performance of the speed-squared controller for the wind turbine.

Fig. 14 and 15 respectively show C_p versus TSR λ and that versus ω_{mech} at different wind speeds. From these two figures, we can point out C_p^{opt}, λ^{opt}, and ω_{mech}^{opt} at different wind speeds. The shape of the curve of C_p is consistent with our analysis in Section 4.1.

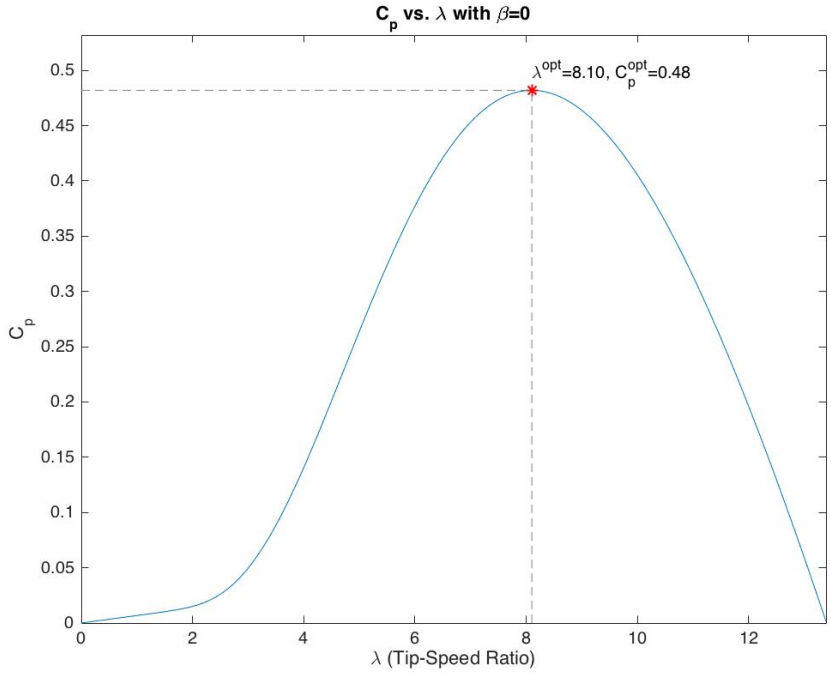

Figure 14: Curve of C_p versus λ

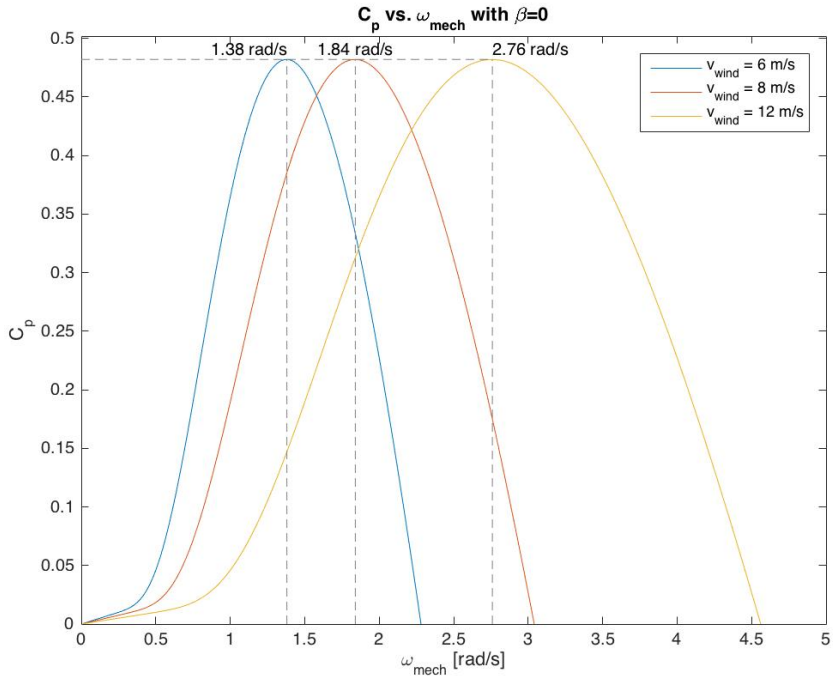

Figure 15: Curve of C_p versus ω_{mech} at Different Wind Speeds

Fig. 16 shows the performance of the speed-squared controller. From the figure, we can find that the controller can effectively adjust the mechanically rotational speed ω_{mech} to remain at the corresponding ω_{mech}^{opt} as the change in v_{wind}.

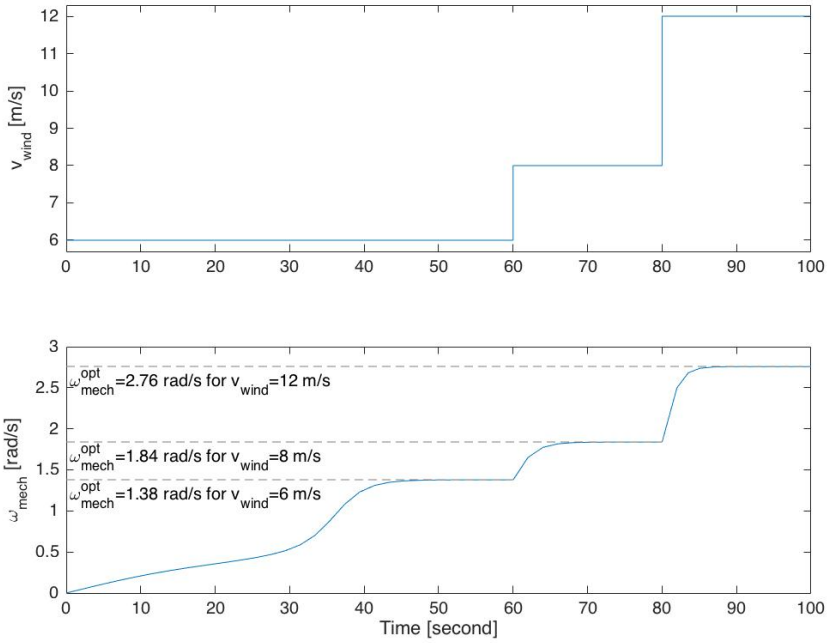

Figure 16: Simulation Results of the Control Performance of the Speed-Squared Controller for Simulation 2

5.2.4 Simulation for the Combined DFIG and Wind Turbine with Certain Wind Speed and Controlled Reference Signal of Q_s

In this simulation, we combine the model of the DFIG and that of the wind turbine together as we described in the former sections.

During the simulation, v_{wind} is set to be 12 m/s. Given that the gear ratio GR is set according to ω_{mech}^{opt} at $v_{wind} = 12$ m/s, the mechanically rotational speed of the DFIG is expected to be its rated value ω_{mech}^{rated}, while the mechanically rotational speed of the wind turbine is expected to be ω_{mech}^{opt} at $v_{wind} = 12$ m/s. From Fig. 15, $\omega_{mech}^{opt} = 2.76$ rad/s when $v_{wind} = 12$ m/s.

In the simulation, Q_s^{ref} decreases from the rated value Q_s^{rated} to 0 at time $t = 30$ s and then increases from 0 to $1.2Q_s^{rated}$ at time $t = 60$ s.

The plot of Q_s, i_{rd}, i_{rq} and their reference signals are shown in Fig. 17. From the figure, it can be recognized that we can effectively generate the reference signal i_{rq}^* through adjusting the reference signal Q_s^* and that Q_s and i_{rq} can be controlled effectively such that they can effectively track their reference signals. On the other hand, we can find that the change in Q_s or say i_{rq} results in the fluctuation of i_{rd} as well as of the actual T_{em} (as shown in Fig. 18). The fluctuation

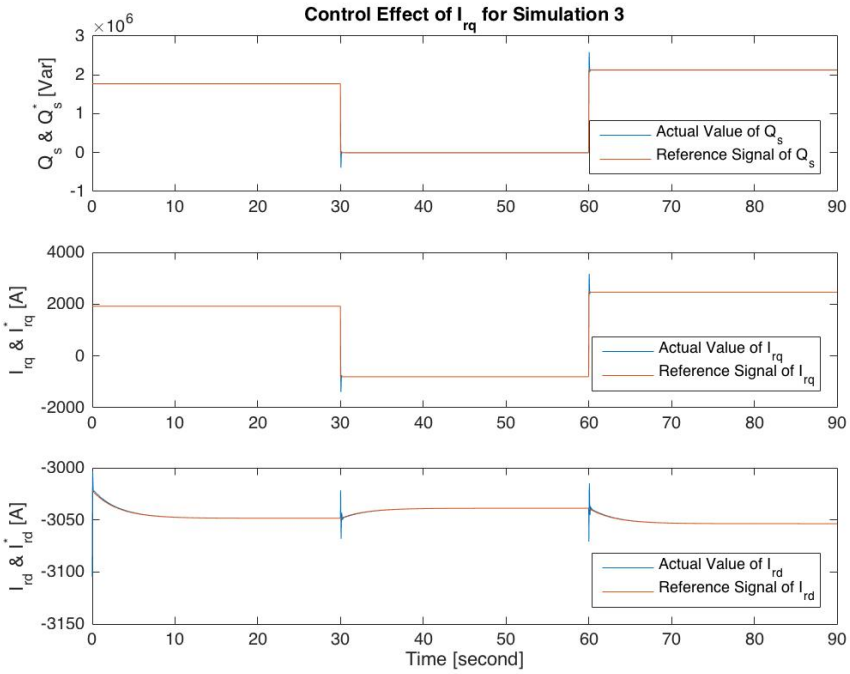

Figure 17: Simulation Results of the Control Effect of i_{rq} for Simulation 3

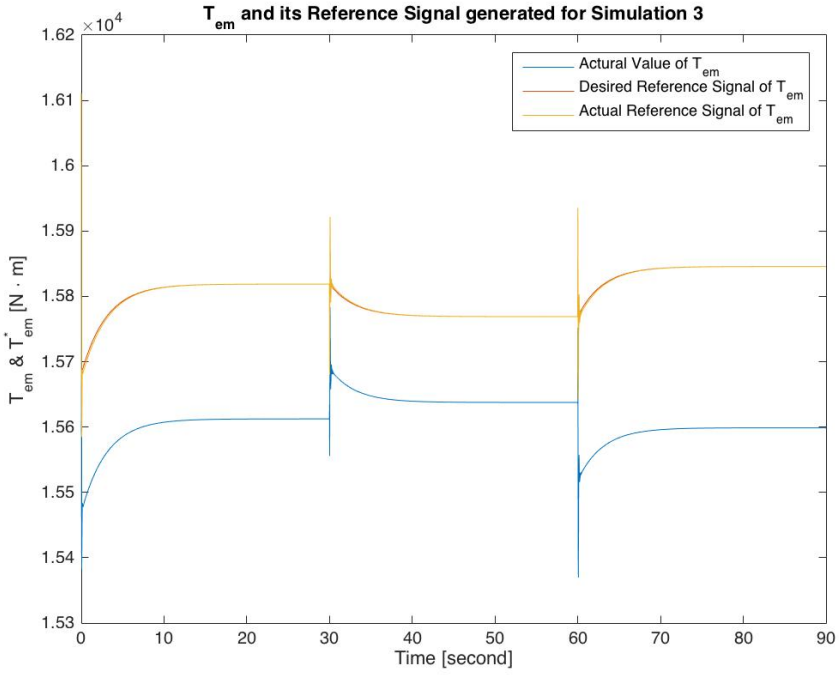

Figure 18: Simulation Results of the T_{em} and its Reference Signal T_{em}^{*} for Simulation 3

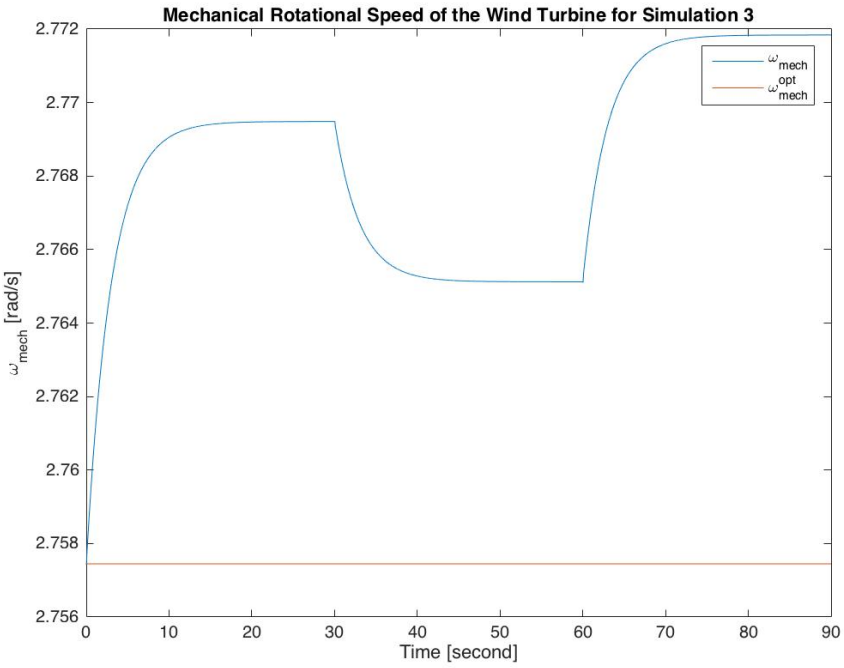

Figure 19: Simulation Results of the Mechanically Rotational Speed of the Wind Turbine for Simulation 3

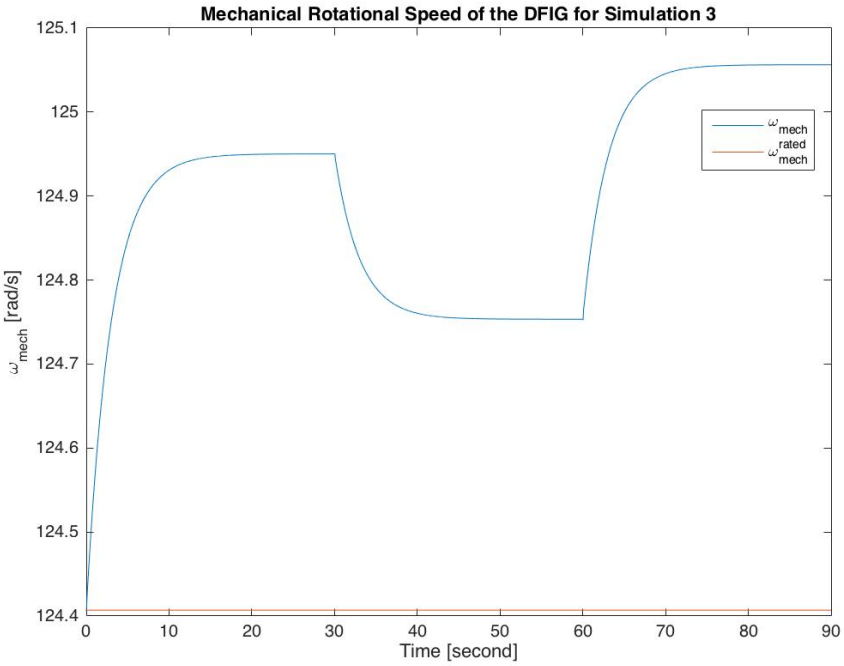

Figure 20: Simulation Results of the Mechanically Rotational Speed of the DFIG for Simulation 3

of T_{em} further leads to the change in the mechanically rotational speed of the wind turbine (as shown in Fig. 19) such that the speed-squared controller leads to the change in i_{rd}^* in order to keep the rotational speed at ω_{mech}^{opt} for $v_{wind} = 12$ m/s. The change of the wind turbine's mechanically rotational speed also is reflected by the mechanically rotational speed of the DFIG, as shwon in Fig. 20.

From Fig. 19 and 20, we can find that the control system does not strictly keep the mechanically rotational speed of the DFIG or that of the wind turbine at its ideal values (ω_{mech}^{rated} and ω_{mech}^{opt} for $v_{wind} = 12$ m/s respectively). However, the gap between the actual value of the ideal value is quite small and acceptable. Hence, the whole control system is still reliable.

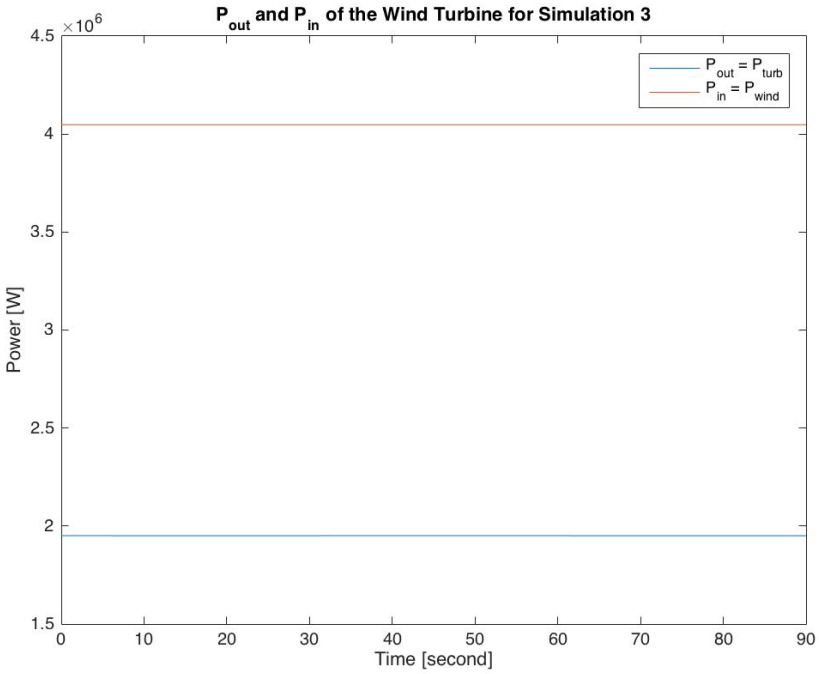

Figure 21: Simulation Results of the Input and Output Power of the Wind Turbine for Simulation 3

Fig. 21 shows the input and output power of the wind turbine. Since v_{wind} is constant in the simulation, the input power P_{wind} is constant as well. Given that the change in the mechanically rotational speed of the wind turbine is quite small, C_p is basically unchanged during the simulation so that there is no change in the output power P_{turb}.

Fig. 22 shows the real and reactive power of the stator and the rotor of the DFIG. From the figure, it can be spotted that P_r is around 0 while $P = P_s + P_r$ is close to the output power of the wind turbine P_{out}.

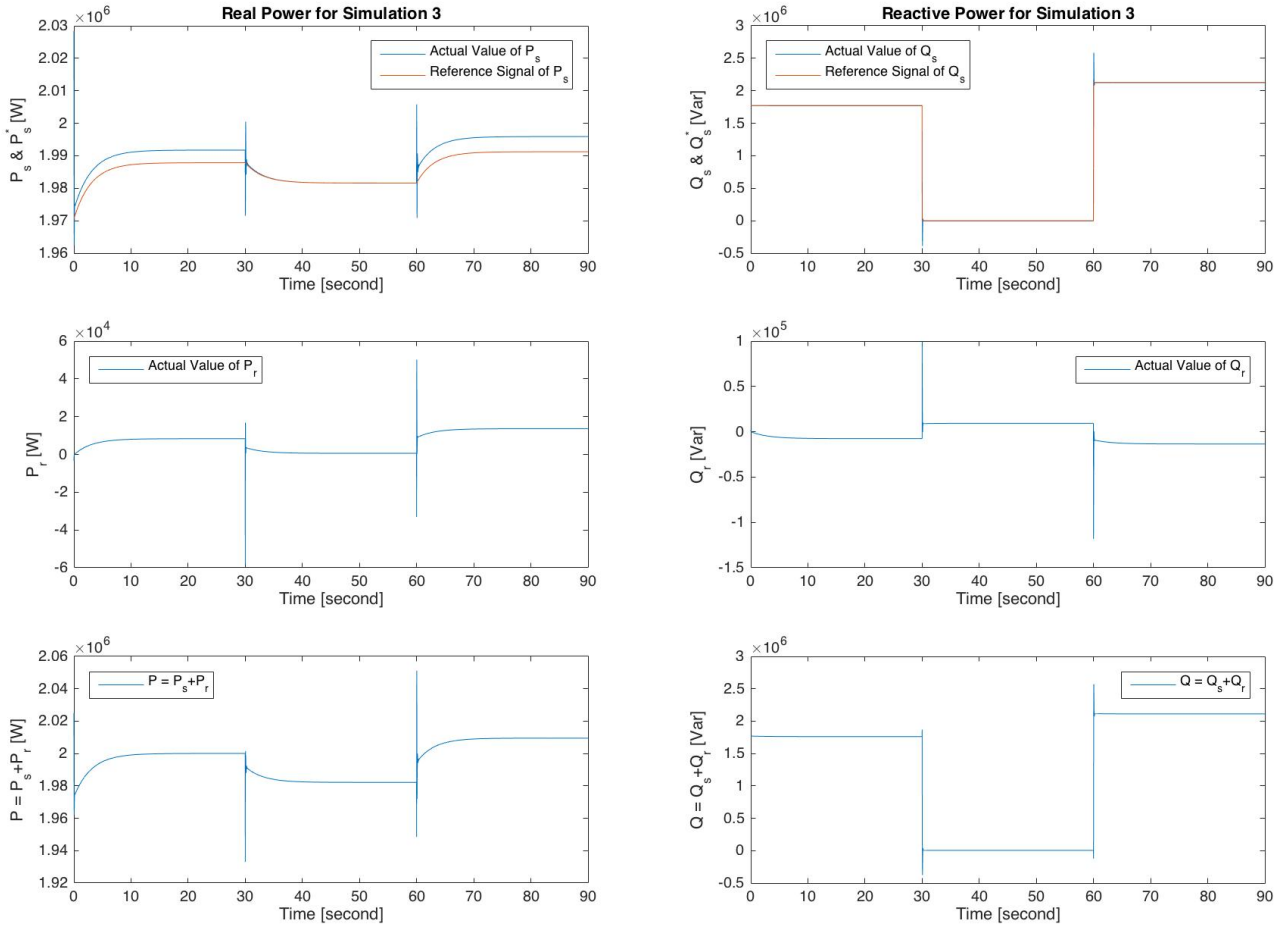

Figure 22: Simulation Results of the Real and Reactive Power of the DFIG for Simulation 3

5.2.5 Simulation for the Combined DFIG and Wind Turbine with Different Wind Speed

In this simulation, Q_s^* is set to be the rated value Q_s^{rated}, whereas the wind speed v_{wind} is changed. And, we hope the control system can adjust the mechanically rotational speed of the wind turbine, ω_{mech}, such that the wind turbines can always run at ω_{mech}^{opt}.

The initial value of v_{wind} is 12 m/s, and the DIFG and wind turbine both operate at the rated condition. Then v_{wind} decreases to 9 m/s at time $t = 30$ s, and then decreases to 6 m/s at time $t = 60$ s.

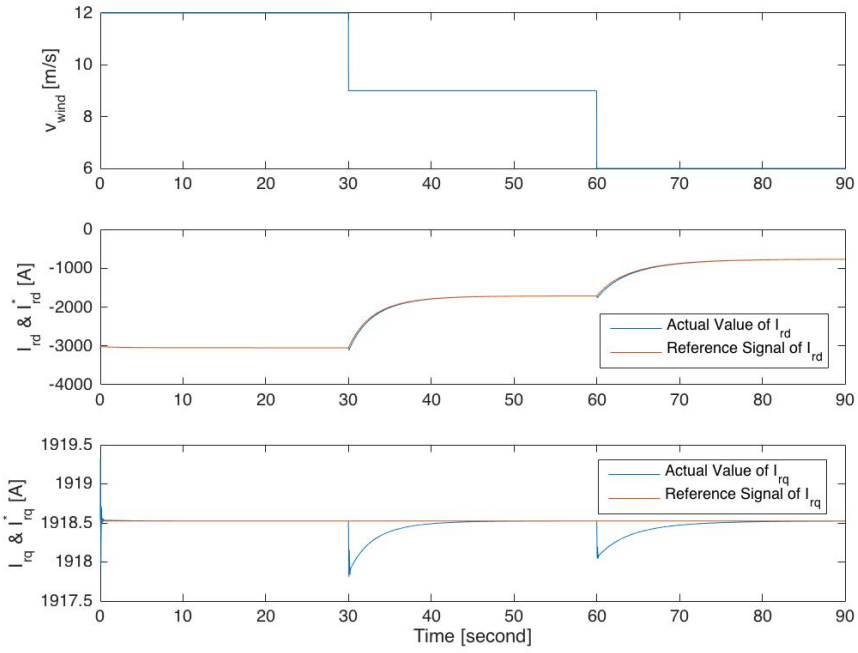

Figure 23: Simulation Results of the Control Effect of i_{rd} for Simulation 4

From Fig. 23, we can spot that as the change in v_{wind}, our control system can rapidly respond and generate the reference signal i_{rd} to control the DFIG's T_{em} (as shown in Fig. 24) and further to control the mechanically rotational speed of the wind turbine (as shown in Fig. 25).

Although the mechanically rotational speed of the wind turbine is controlled to keep at ω_{mech}^{opt} according to the different wind speed, as shown in Fig. 25, the mechanically rotational speed of the DFIG is not always keep at its rated value ω_{mech}^{rated}, as shown in Fig. 26 Given that the gear ratio is set according to the ratio of ω_{mech}^{rated} and ω_{mech}^{opt} at $v_{wind} = 12$ m/s, only when $v_{wind} = 12$ m/s can the mechanically rotational speed of the DFIG be kept at or say close to ω_{mech}^{opt}.

Besides, from Fig. 26, the mechanically rotational speed of the DFIG change dramatically as the wind speed changes. Due to the characteristic of the DFIG, DFIG can run in a sufficiently wide speed range so that it usually is adaptable to the dramatic change in the mechanically rotational speed.

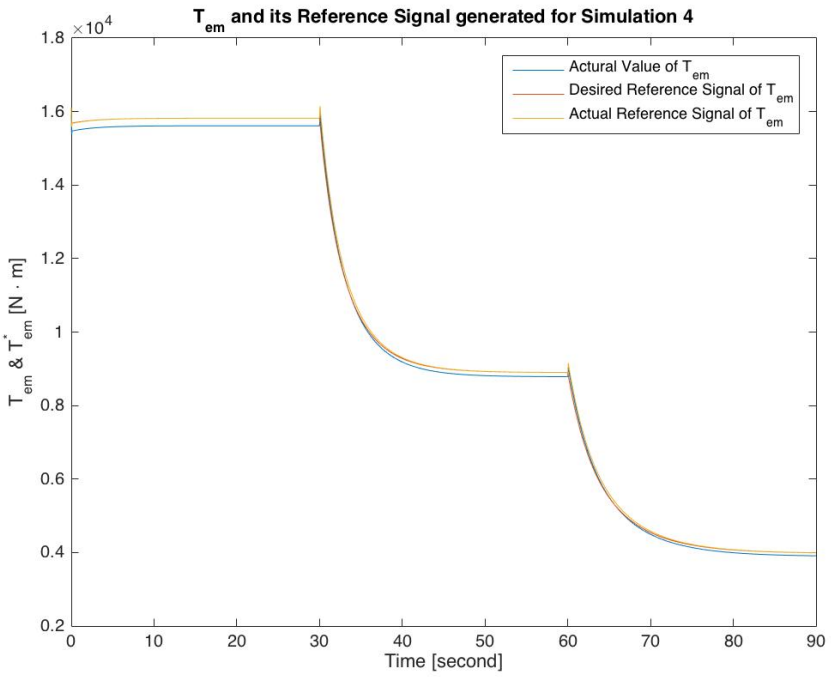

Figure 24: Simulation Results of the T_{em} and its Reference Signal T_{em}^{*} for Simulation 4

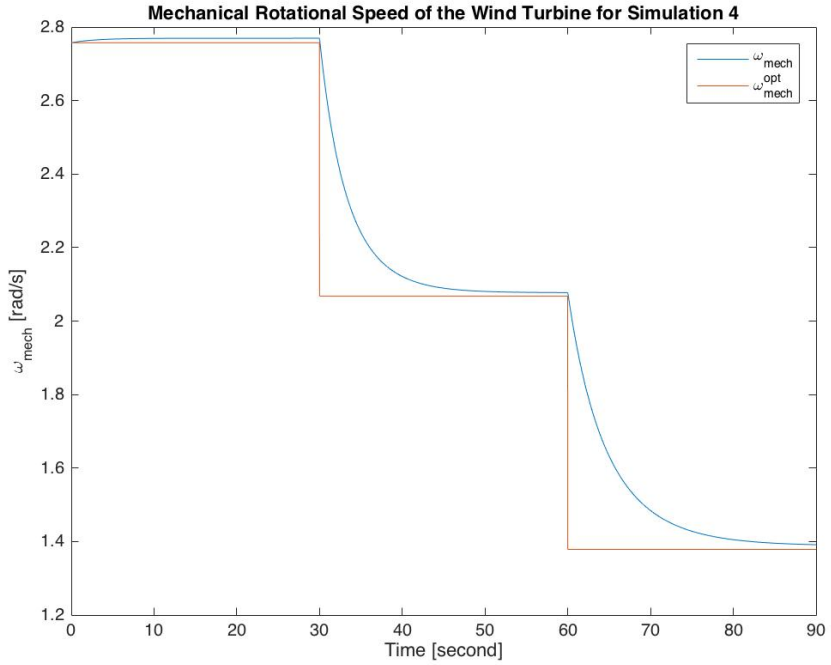

Figure 25: Simulation Results of the Mechanically Rotational Speed of the Wind Turbine for Simulation 4

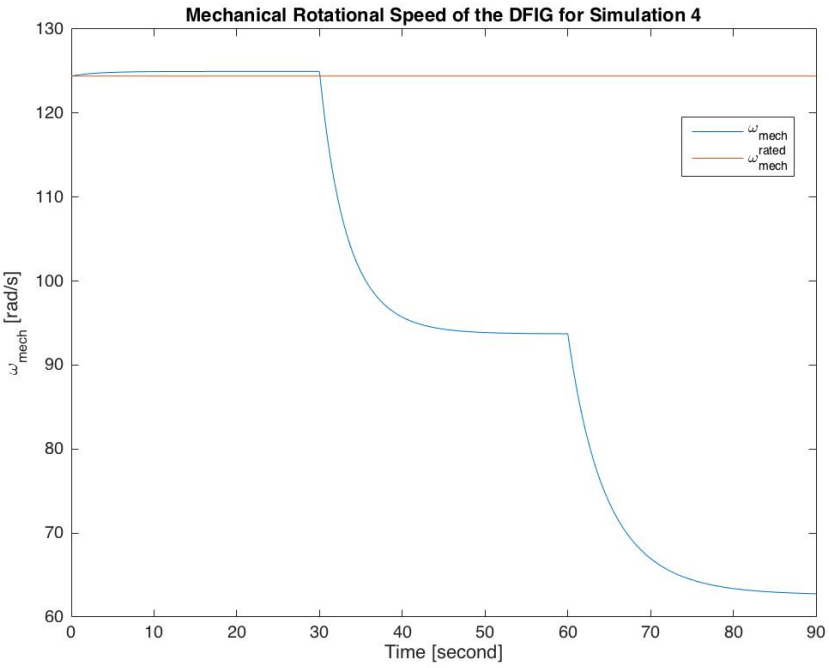

Figure 26: Simulation Results of the Mechanically Rotational Speed of the DFIG for Simulation 4

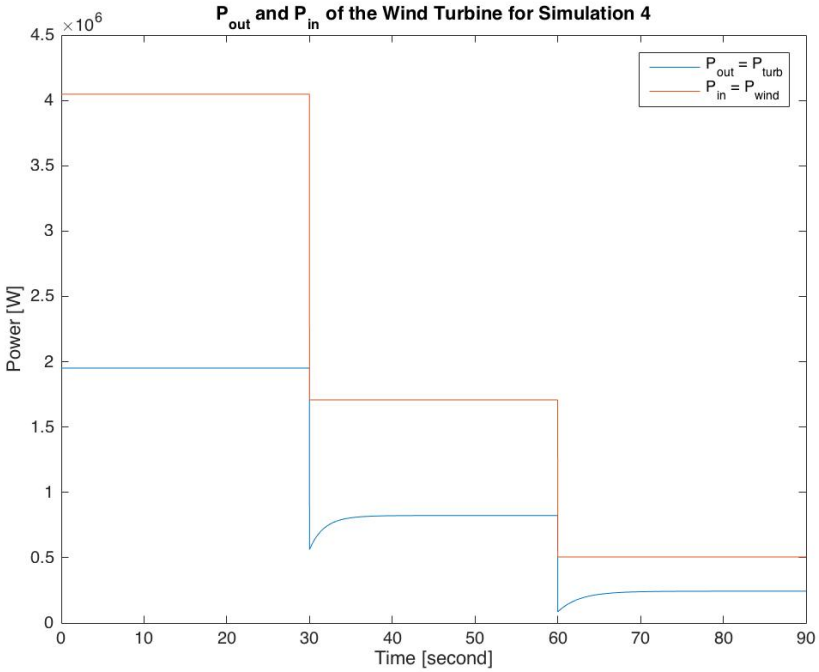

Figure 27: Simulation Results of the Input and Output Power of the Wind Turbine for Simulation 4

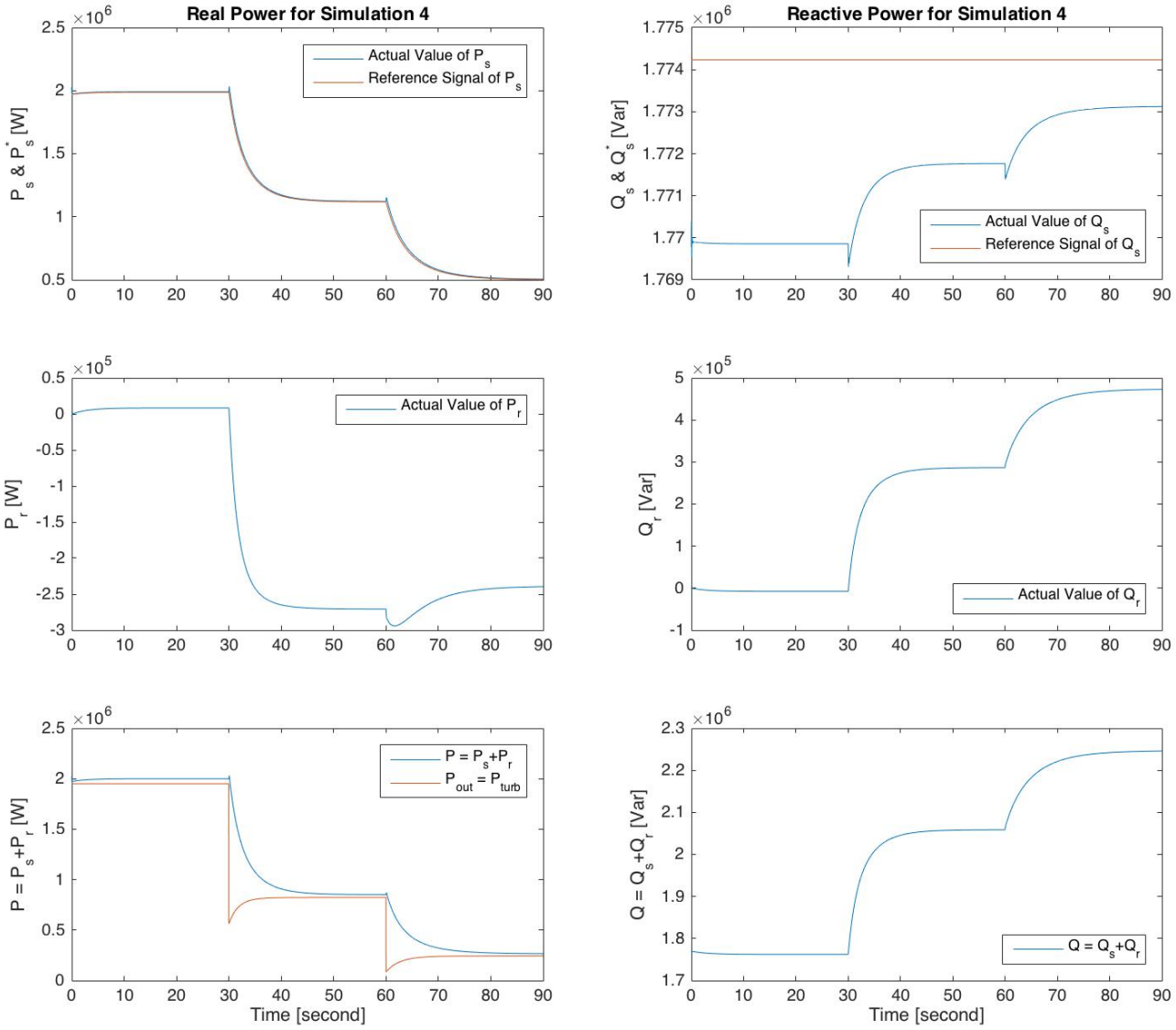

Figure 28: Simulation Results of the Real and Reactive Power of the DFIG for Simulation 4

Fig. 27 shows the input and output power of the wind turbine. Fig. 28 shows the real and reactive power of the DFIG. From the 5th plot in Fig. 28, we can find that in steady state $P_{turb} \approx P_s + P_r$. This demonstrates that the power outputted by the wind turbine is consumed by both of rotor and stator.

6 Conclusion and Discussion

In this project, the model of doubly fed induction generator (DFIG) and wind turbine in dq domain and the model of the related controllers are built up in theory as well as in MATLAB/Simulink. From simulation, it is proven that the designed controllers can effectively control DFIG and also can automatically adjust the rotor voltage applied to the DFIG and thus make the wind turbine operate at a optimal condition.

From the analysis in Section 5.2.5, we find that

$$P_{turb} \approx P_s + P_r \tag{6.97}$$

where P_{turb} is the output real power of the wind turbine and P_s and P_r are the real power of the DFIG's stator and rotor respectively. That is to say, the wind turbine's output power is consumed by both of stator and rotor.

From the analysis in Section 5.2.2, although the change in Q_s could make i_{rd} fluctuate and thus cause some fluctuation of P_s and T_{em} who are associated with i_{rd} and some other constants, the fluctuation is very small and these quantities would recover rapidly. Similarly, although the change in i_{rd} could make i_{rq} as well as Q_s fluctuate, the influence is quite small and Q_s can be effectively modulated through the reference signal we give. This conclusion also is demonstrate via Fig. 12, 17 22 and 28 in which the actual value of Q_s can effectively follow the reference signal Q_s^*.

From Fig. 19 and Fig. 25, although with the control system, the wind turbine's mechanically rotational speed could be close to the optimal speed ω_{mech}^{opt}, which is decided by the wind speed v_{wind}, there still is a gap between the ideal ω_{mech}^{opt} and the actual ω_{mech}. This gap is mainly caused by our neglect of R_s, R_r, L_{lr} and L_{ls} in the process of modeling the DFIG. The actual ω_{mech} is a little bigger than the ideal ω_{mech}^{opt}. For $v_{wind} = 12$ m/s, $\omega_{mech} = 2.769$ rad/s in steady state; for $v_{wind} = 9$ m/s, $\omega_{mech} = 2.078$ rad/s in steady state; and for $v_{wind} = 6$ m/s, $\omega_{mech} = 1.393$ rad/s in steady state. These data are obtained from Fig. 25.

When the mechanically rotational speed is the rated speed ω_{mech}^{rated}, the slip of the DFIG is its rated value or the value with full load, i.e. 0.01. However, since the gear ratio is set to be the ratio of ω_{mech}^{rated} to the optimal mechanically rotational speed of the wind turbine at $v_{wind} = 12$ m/s, only when the mechanically rotational speed of the wind turbine is the ω_{mech}^{opt} at $v_{wind} = 12$ m/s can the slip is its rated value. However, due to the existence of the gap between the mechanically rotational speed of the wind turbine and the optimal speed (as mentioned in the last paragraph), the slip is smaller than 0.01 even if $v_{wind} = 12$ m/s. For $v_{wind} = 12$ m/s, the slip is 0.005; for $v_{wind} = 9$ m/s, the slip is 0.25; and for $v_{wind} = 6$ m/s, the slip is 0.50. These data can be calculated from the mechanically rotational speed of the wind turbine or that of the DFIG.

Besides, as our analysis in Section 3.2, v_{sd} should be a constant and v_sq should be zero. However, in our model, there exists oscillation of v_{sd} and v_{sq}, as shown in Fig. 29. Although the amplitude

of the oscillation is quite small, I wonder if it could influence the control effect on the DFIG. The reason causing the oscillation and the influence of the oscillation may be focused on in the next phase of learning.

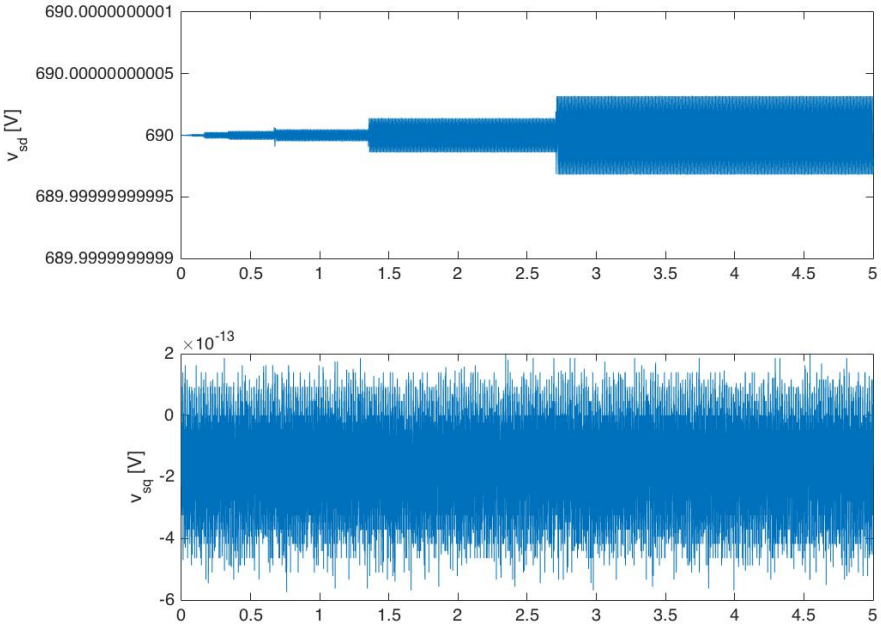

Figure 29: v_{sd} and v_{sq} Generated

Additionally, as our analysis in Section 5.2.4 and 5.2.5, there is a gap between our desired reference of the reference signal T^*_{em} generated through adjusting the reference signal i^*_{rd}, as shown in Fig. 18 and 24. This gap exists due to that R_s, R_r, L_{ls} and L_{lr} are not really zero and thus that there in fact is no strictly proportional relationship between T_{em} and i_{rd}. In summary, although our control system cannot accurately control the electromagnetic torque of the DFIG as well as the mechanically rotational speed of the wind turbine, the control effect is acceptable. Therefore, it is effective to use the controller designed according to the approximation relation between T_{em} and i_{rd} and that between Q_s and i_{rq}.

References

[1] N. Mohan, *Electric Machines and Drives*. 2012.

[2] N. Mohan, *Advanced Electric Drives: Analysis, Control, and Modeling Using MATLAB/Simulink®*. 2014.